AEROSOL SCIENCE AND TECHNOLOGY
2023, VOL. 57, NO. 8, 713–726
https://doi.org/10.1080/02786826.2023.2211121

Parameterization of polydisperse aerosol optical properties during hygroscopic growth

Chang H. Jung[a], Kyung Man Han[b], Young Jun Yoon[c], Dongchul Kim[d,e], Ji Yi Lee[f], Hyung-Min Lee[f], Junshik Um[g,h], Seoung Soo Lee[i,j,k], and Yong Pyo Kim[l]

[a]Department of Health Management, Kyungin Women's University, Incheon, Korea; [b]School of Earth Sciences and Environmental Engineering, Gwangju Institute of Science and Technology, Gwangju, Korea; [c]Korea Polar Research Institute, Incheon, Korea; [d]University of Maryland, Baltimore County, Baltimore, Maryland, USA; [e]NASA Goddard Space Flight Center, Greenbelt, Maryland, USA; [f]Department of Environmental Science and Engineering, Ewha Womans University, Seoul, Korea; [g]Department of Atmospheric Sciences, Division of Earth Environmental System, BK21 School of Earth and Environmental Systems, Pusan National University, Busan, Korea; [h]Institute of Environmental Studies, Pusan National University, Busan, Korea; [i]Earth System Science Interdisciplinary Center, University of Maryland, College Park, Maryland, USA; [j]Research Center for Climate Sciences, Pusan National University, Busan, Korea; [k]Science and Technology Corporation, California, USA; [l]Department of Chemical Engineering and Materials Science, Ewha Womans University, Seoul, Korea

ABSTRACT

Aerosol water uptake and the related influence on its optical properties owing to the hygroscopic growth of polydisperse aerosols have a significant effect on air quality and climate. This study develops an analytical parameterization for a single hygroscopic optical parameter and the scattering enhancement factor for polydisperse aerosol sizes. Polydisperse lognormal size distributions for geometric mean diameters of 0.05–1 μm and geometric standard deviations of 1.3–2.5 are considered with real refractive indices between 1.35 and 1.6. The analytical expression obtained for the optical parameter is compared to Mie theory and reasonable agreements within the size range investigated in this study are observed. Further, our results show that the analytical expression could express polydispersed aerosol optical properties as a function of geometric mean diameter and geometric standard deviation of a lognormal distribution and the refractive index. The obtained analytical expression can be efficiently used for 3D models with a reduced computational burden.

ARTICLE HISTORY
Received 21 September 2022
Accepted 30 April 2023

EDITOR
Hans Moosmüller

1. Introduction

The hygroscopic growth of aerosols is related to meteorological, chemical, and physical properties (Junge and McLaren 1971; Shulman et al. 1996; McFiggans et al. 2006; Petters and Kreidenweis 2007). The aerosol hygroscopic growth factor indicates the relative increase in the mobility diameter of particles due to water absorption at a specific relative humidity (RH). Prediction of hygroscopic growth factors require detailed knowledge of particle chemical composition and a thermodynamic model, which describes the concentration dependence of the water (Eichler et al. 2008; Kreidenweis et al. 2008; Laskina et al. 2015; Sorooshian et al. 2008; Wexler and Clegg 2002).

The growth factor (GF) attributed to aerosol hygroscopic growth can be specified by following Equation (1).

$$GF(RH) = \left(\frac{V_{wet}(RH)}{V_s}\right)^{1/3} = \left(\frac{V_s + V_w(RH)}{V_s}\right)^{1/3} = \left(1 + \frac{V_w(RH)}{V_s}\right)^{1/3} \quad (1)$$

where $V_{wet}(= V_s + V_w)$, V_s, and V_w are the volumes of wet aerosol, dry aerosol, and water, respectively. According to Petters and Kreidenweis (2007), aerosol hygroscopic growth can be approximated using the single hygroscopicity parameter (κ) and water activity (a_w). The relation is expressed as follows:

$$\frac{1}{a_w} = 1 + \kappa\frac{V_s}{V_w} \quad (2)$$

Here, a_w is the water activity in the solution and can be replaced by RH, if the Kelvin effect is omitted.

CONTACT Chang H. Jung jch@kiwu.ac.kr

Supplemental data for this article can be accessed online at https://doi.org/10.1080/02786826.2023.2211121.

The Kelvin effect becomes negligible for particles larger than 50 nm in radius. Many studies justify the replacement of water activity with RH (Kuang et al. 2017; Li et al. 2014; Park and Lee 2000; Seinfeld and Pandis 2016; Topping et al. 2005; Zhao et al. 2022; Zieger et al. 2010).

It should be noted that κ is widely used in studies of aerosol hygroscopic growth and cloud condensation nucleus activation (Petters and Kreidenweis 2007; Yu et al. 2018; Zhao et al. 2022). From Equation (2), V_w can be expressed as follows (Petters and Kreidenweis 2007), disregarding the Kelvin (curvature) effects (RH = a_w) (Park and Lee 2000):

$$V_w = V_s \frac{\kappa RH}{100 - RH} \tag{3}$$

Water uptake by aerosol particles significantly influences aerosol optical properties and climate (Horvath 1996; Haywood and Boucher 2000).

The quantification of the scattering enhancement factor, f(RH), is essential for determining the response of aerosol optical properties to hygroscopic growth at various ambient RH conditions.

The f(RH) can be introduced to quantify the effect of hygroscopic growth on aerosol scattering.

Here, f(RH) is defined as the ratio of scattering coefficient for dry and wet aerosol at enhanced RH conditions (Covert et al. 1972; Lagrosas et al. 2019; Pitchford et al. 2007; Zhang et al. 2014; Zieger et al. 2010):

$$f(RH) = \frac{b_{sca}(RH)}{b_{sca}(dry)} \tag{4}$$

where b_{sca}(RH) and b_{sca}(dry) are the aerosol light scattering coefficients under RH and dry conditions, respectively. When RH <40%, we assume the dry aerosol with no water uptake and f(RH) is 1 (Covert et al. 1972; Chen et al. 2014; Pitchford et al. 2007). Several measurement stations, such as those involved in the ACTRIS or GAW (WMO/GAW, 2003) networks, perform routine measurements of aerosol optical and physical properties at dry conditions (RH <40%) (Titos et al. 2016).

One of the important characteristics of b_{sca} is polydispersity. b_{sca} can be expressed as a function of particle size and refractive index (m).

$$b_{sca} = \int_0^{d_{p,\max}} Q_{sca}(d_p, m) \frac{\pi}{4} d_p^2 n(d_p) \delta d_p \tag{5}$$

where $Q_{sca}(d_p, m)$, $d_{p,\max}$, and δ represent the single particle scattering efficiency, maximum particle diameter, and derivative symbol, respectively (Seinfeld and Pandis 2016). All the optical properties calculated in this study are at a wavelength of 550 nm.

f(RH) values are influenced by the aerosol number size distribution, wavelength, and chemical composition corresponding to refractive index and hygroscopicity (Zieger et al. 2013). Here, the aerosol refractive index is closely related to aerosol composition (Chen et al. 2014).

For a given RH and chemical composition, different aerosol size distributions should yield different f(RH) (Molnár et al. 2020; Pitchford et al. 2007). Under the lognormal aerosol size distribution assumption, f(RH) should be expressed as a function of aerosol geometric mean diameter (d_{g0}) and geometric standard deviation (GSD) of dry aerosol. Previous studies often have neglected the effect of size distribution on f(RH) (Malm et al. 1994; Han et al. 2021). Malm et al. (1994) developed IMPROVE (Interagency Monitoring of Protected Visual Environments) algorithm for estimating light extinction by using reconstructed method. The effects of the uptake of water are estimated by the f(RH) as a function of relative humidity (RH). Malm et al. (1994) did not consider aerosol size distribution. Pitchford et al. (2007) revised the IMPROVE equation for small- and large-mode particles with associated f(RH). Although Pitchford et al. (2007) consider small and large mode particles in estimating f(RH), the effect of polydisperse size distribution cannot be estimated. Jung et al. (2021) developed an approximate formula for the f(RH) of a polydisperse size distribution of ammonium sulfate and NaCl from the computed mass growth factors based on aerosol thermodynamic models using Mie theory. Their study had difficulty dealing with various internally mixed aerosols. Thus, simple parameterizations of hygroscopic growth factors for polydisperse aerosols are useful and challenging instead of adopting a complicated numerical approach (Jung et al. 2021).

One way to parameterize f(RH) is based on a single hygroscopic optical parameter (κ_{sca}) (Brock et al. 2016; Yu et al. 2018). This parameterization scheme estimates f(RH) as a function of RH and κ_{sca}. Brock et al. (2016) developed a parameterization for f(RH) from κ-Köhler and Mie theories. This parameterization is given by

$$f(RH) = 1 + \kappa_{sca} \frac{RH}{100 - RH} \tag{6}$$

Here, the fitted parameter, κ_{sca}, is useful because it is a single optical parameter for hygroscopicity and is related to κ. However, determining κ_{sca} at a given κ for polydisperse size using Mie theory is numerically complex and computationally expensive.

In this study, we analytically parameterized κ_{sca} and f(RH) for polydisperse aerosol sizes. Here κ_{sca} can

be fitted based on Mie calculations. The effects of refractive indices and lognormal size distribution were considered. The parameterized κ_{sca} and f(RH) were compared with results calculated using Mie theory, with different size distribution parameters. The hygroscopic properties of current parameterization and existing reconstructed expression were compared with each other from the 3-D Weather Research & Forecasting Model/Community Multiscale Air Quality Modeling (WRFv3.8.1/CMAQv5.2.1) simulation.

2. Methods

2.1. Aerosol mixing state

In estimating aerosol hygroscopicity, the assumption of the mixing state is critical. Usually, the aerosol mixing state in the ambient atmosphere ranges between the external mixture, where each particle is composed of a single species, and an internal mixture, where all particles are assumed to be the same chemical composition. Many studies quantified the importance of mixing states for aerosol optical properties through optical closure studies (Koike et al. 2014; Yu et al. 2018). The internal mixture assumption is generally known to lead to an underestimation of the volume scattering coefficients. The relative errors for the scattering coefficient, for example, reached up to −32%. (Yao et al. 2022). Erlick et al. (2011) used the core-shell assumption to calculate how the optical properties of internally-mixed brown carbon-inorganic particles differed between liquid-liquid phase separated particles and homogeneously-mixed particles. The maximum relative difference in the single scattering albedo was 25% (Fard et al. 2018; Stevens and Dastoor 2019).

In spite of these discrepancies between mixing assumptions, many studies rely on simplifying assumptions of aerosol mixing state for computational efficiency (Yao et al. 2022). In this study, we investigated aerosol hygroscopicity based on the internally mixed aerosol assumption. The hygroscopicity parameter (κ) to simplify the complex physicochemical properties of particle hygroscopicity (Petters and Kreidenweis 2007) is introduced. Based on the ZSR mixing rule (Stokes and Robinson 1966; Zdanovskii 1948), κ of multicomponent aerosol particles is obtained by the volume-weighted κ of every single component (Levin et al. 2014; Petters and Kreidenweis 2007; Yu et al. 2018).

$$\kappa = \sum_i \varepsilon_i \kappa_i \tag{7}$$

where κ_i and ε_i are the hygroscopicity parameter and volume fraction of the *ith* individual components, respectively. Typically, an internally mixed continental aerosol is assumed to have a representative hygroscopicity parameter, κ, of 0.3 (Levin 2014; Wang et al. 2018). Organic aerosols usually have lower κ (Petters and Kreidenweis 2007). For example, Shingler et al. (2016) reported κ values for different air mass types as 0.12 for agricultural burning, 0.11 for wildfires, 0.21 for biogenic, and 0.28 for urban aerosol. κ values for marine aerosols have been reported to be larger than continental aerosols. κ values for pure sea salt could be as much as 1.24 (Almeida et al. 2019; Cuevas-Robles et al. 2021). It should be noted that the volume does not change by mixing because all the properties regarding particle mixings are based on volume-weighted assumptions.

2.2. Refractive index

The complex refractive index is fundamental to aerosol optical parameters such as the single scattering albedo and asymmetry parameter. Knowing the value of the refractive index is critical in modeling the optical properties of aerosols and predicting radiative forcing on regional and global scales. The real (m_r) and imaginary (m_i) parts of the refractive index indicate scattering and absorption, respectively, which are determined by the particles' chemical composition (He et al. 2018). There are many previous studies regarding the range of the aerosol refractive index. For example, past measurement studies of ambient aerosol particles have reported a wide range of m_r values, usually between 1.4 and 1.6 (e.g., Dubovik et al. 2002; Ferrare et al. 1998; Guyon et al. 2003; Wang and Rood 2008). Some other studies reported the range of m_r values for secondary organic aerosol as 1.35–1.6 (Moise et al. 2015). According to Bain et al. (2019), the complex refractive index of aqueous salt solutions has a m_r between 1.3 and 1.6 and an m_i that is typically on the magnitude of 10^{-9} to 10^{-6} at optical frequencies. Both the m_r and m_i vary with wavelength. The m_i is largely ignored when discussing aqueous atmospheric aerosol particles and is usually set to 0 in calculations. According to Jurányi and Weller (2019), the highest possible estimate of the error we make if we would neglect the m_i never exceeds 1.7 % when considering $4 \times 10^{-3}i$ instead of $0.0i$. In this study, we ignored the imaginary part of the refractive index.

As a particle becomes larger by taking up water at higher RH, it will become more dilute, and the index of refraction will become closer to that of water (∼1.33 at 550 nm, Seinfeld and Pandis 2016). In this

study, the dilution effects of the refractive index and related changes in optical properties are considered. The effective refractive index for a mixture of aerosols can be calculated by using the values of the complex refractive index and the volume fraction of each aerosol component or the volume averaging mixing rule. It is assumed that all the specific components of aerosols make a homogenous mixture (Levoni et al. 1997; Mico et al. 2019).

$$m_r(RH) = \frac{m_{r,Dry}V_s + n_{r,w}V_w(RH)}{V_s + V_w(RH)} \quad (8)$$

where $m_r(RH)$, $m_{r,Dry}$ and $n_{r,w}$ are the refractive index at RH, dry aerosol and water, respectively.

Figure 1 shows the change in the m_r(RH) and $d_g(RH)/d_{g0}$ as a function of RH. κ of 0.1, 0.3, and 0.5 are compared. As shown in Figure 1a, the refractive index, which was initially 1.4, 1.5, and 1.6, respectively, decreases and approaches 1.33 as RH increases. The decreasing tendency strengthens as κ increases because of increasing water content. Figure 1b shows that d_g increase as RH increases because of dilution with water. Figure 1b also exhibits that $d_g(RH)/d_{g0}$ increases as κ increases.

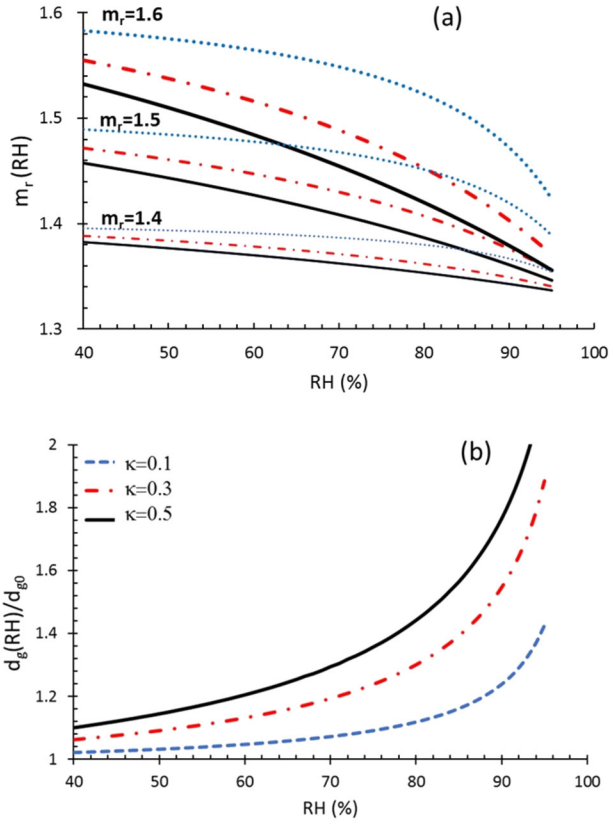

Figure 1. Changes in the (a) real refractive index (m_r(RH)) and (b) ratio between wet aerosol geometric mean diameter at RH and dry aerosol geometric mean diameter ($d_g(RH/)d_{g0}$) as a function of RH for different κ (40% < RH < 95%) (·····: $\kappa = 0.1$; – · –: $\kappa = 0.3$; ——: $\kappa = 0.5$).

2.3. Procedure for the parameterization

Figure 2 shows the schematic for the acquisition and parameterization of the κ_{sca} and f(RH) for polydisperse aerosols. A summary of the procedure for this study is provided below. Based on a given GSD, d_{g0}, and refractive index, the b_{ext}(dry) can be calculated using Mie theory. Here we assumed the wavelength of visibility (550 nm). Mie scattering code in this study is based on the BHMIE subroutine for calculating scattering and absorption by spheres (Bohren and Huffman 1983). Aerosol absorption was neglected and then the extinction coefficient (b_{ext}) is assumed to be identical to the scattering coefficient ($b_{ext} = b_{sca}$). We can calculate the new wet aerosol size distribution due to the addition of water and hygroscopic growth.b_{sca}(RH) was calculated based on Mie theory using the wet size distribution and refractive index, which accounts for the change in particle volume and refractive index due to the addition of water. The volume of water (V_w) can be calculated from Equation (3) at a given κ and RH. Here, we assumed that the aerosol size retained a lognormal size distribution and GSD is invariant under the assumption that the change of GSD is relatively marginal compared with the change of d_{g0}. Such an assumption is generally helpful for computational stability because of its simplicity (Binkowski, 1999; Binkowski and Roselle 2003). The degree of hygroscopicity depends on the composition. This assumption is applicable under the internal mixing assumption. From the calculated f(RH) for polydisperse aerosol sizes based on Equations (4) and (5), κ_{sca} can be fitted and parameterized as a function of the size distribution parameter using a refractive index *via* multilinear regression in the range of RH 40–95%. A detailed description of the size-resolved analytic parameterization of κ_{sca} is provided in Section 2.4.

The size dependency of the hygroscopic growth factor of the particle in the range of d_{g0} of 0.05–1 μm with GSD of 1.3–2.5 was investigated (Table 1). The variation in m_r was also considered within the range of 1.35–1.6 at the wavelength of 550 nm. We consider various κ of 0.1, 0.3, 0.5, 0.7, and 1.24.

For the application, we used meteorological information and aerosol concentrations obtained from WRFv3.8.1/CMAQv5.2.1 model simulations (Byun and Schere 2006). The simulation periods for model running were during the six weeks (01 May 2016 to 12 June 2016) of the KORUS-AQ (a joint Korea-United States Air Quality Study) campaign (Crawford et al. 2021). In the simulation, the grid spacing is

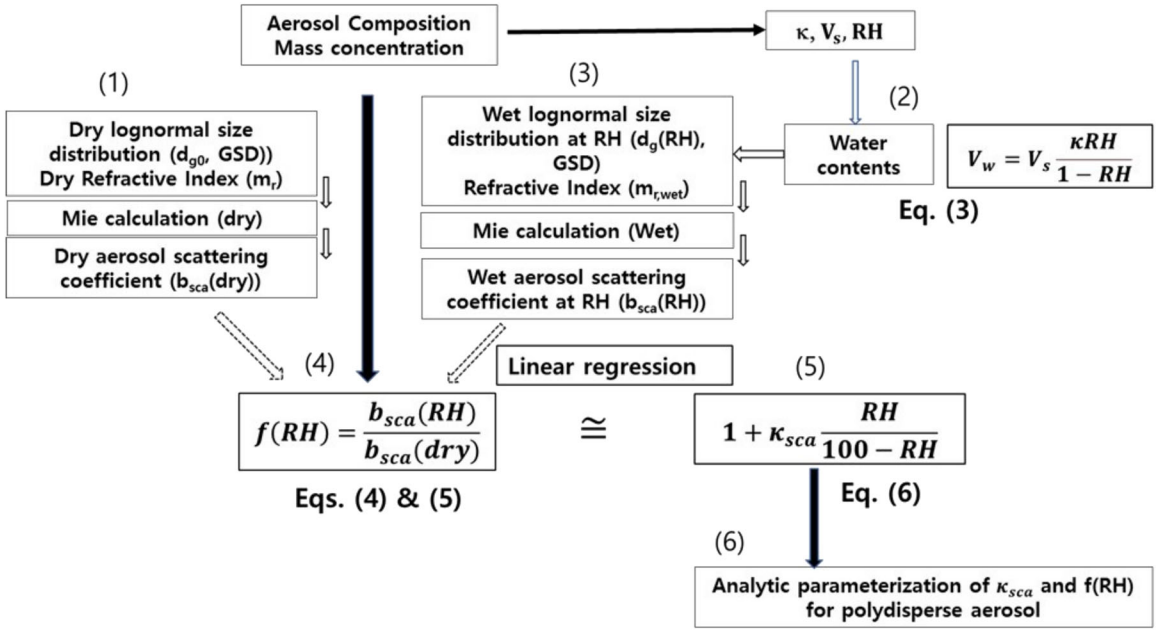

Figure 2. Stepwise process for the parameterization of κ_{sca} and f(RH).

Table 1. Experimental conditions for study cases (at the dry aerosol condition).

Parameter	Case	Unit
Single hygroscopicity parameter (κ)	0.1, 0.3, 0.5, 0.7, 1.24	–
Dry aerosol geometric mean diameter (d_{g0})	0.05–1.0 (15-point, 7-point, 4-point)	μm
Geometric standard deviation (GSD)	1.3, 1.5, 1.7, 1.9, 2.1, 2.3, 2.5	–
Dry aerosol real refractive index (m_r)	1.35, 1.4, 1.45, 1.5, 1.55, 1.6	–

15 km × 15 km horizontally and 17 vertical sigma levels with the model top at 50 hPa. For the input of emission data, the simulation took into account the KORUS v5.0 (https://aisl.konkuk.ac.kr/#/emission_data/korus-aq_emissions), MEGAN-MACC (https://eccad.aeris-data.fr/), and FINNv1.5 (https://www.acom.ucar.edu/Data/fire/) inventories for anthropogenic, biogenic, and fire emission sources, respectively. Other detailed model configurations were discussed by Han et al. (2021).

2.4. Analytic parameterization of size-resolved κ_{sca} and f(RH)

If the aerosol size distribution is assumed to be lognormal, κ_{sca} at a given κ can be expressed as a function of m_r, d_{g0}, and GSD of dry aerosol.

$$\kappa_{sca} = g(m_r, d_{g0}, \ GSD) \tag{9}$$

We propose the analytic expression of κ_{sca} using simple parameterizations. First, the calculated κ_{sca} for polydisperse aerosols can be fitted as a power function of d_{g0}.

$$\kappa_{sca} = a \times {d_{g0}}^{b} \tag{10}$$

where a and b are coefficients for fitting κ_{sca} at different GSD, m_r, and κ values.

Second, based on Mie-based calculations, a and b can be linearly approximated as a function of GSD for a given m_r and κ.

$$\begin{aligned} a &= a_1 GSD + a_2, \\ b &= b_1 GSD + b_2 \end{aligned} \tag{11}$$

Here, a_1, a_2, b_1, and b_2 can be approximated as functions of m_r. Subsequently, the resulting analytic formulae of κ_{sca} for the polydispersed aerosol were expressed as a function of the d_{g0} and GSD by combining Equations (10) and (11) as follows:

$$\kappa_{sca} = (a_1 GSD + a_2) {d_{g0}}^{(b_1 GSD + b_2)} \tag{12}$$

In Equation (12), coefficients can be expressed as a function of m_r.

$$\begin{aligned} a_1 &= a_{11} m_r + a_{12}, \\ a_2 &= \mathrm{C}, \\ b_1 &= b_{11} m + b_{12}, \\ b_2 &= b_{21} m_r + b_{22} \end{aligned} \tag{13}$$

where a_{11}, a_{12}, b_{11}, b_{12}, b_{21}, and b_{22} are the fitted coefficients representing a_1, b_1, and b_2 as a function of m_r from the linear regression. a_2 is a constant (C). Here, we approximated the coefficients as a function

Table 2. Summary of the resultant approximation of κ_{sca} for different values of κ (0.1, 0.3, 0.5, 0.7, and 1.24). ($\kappa_{sca} = (a_{11} \times m_r + a_{12}) \times GSD + a_2) \times d_g^{((b_{11} \times m_r + b_{12}) \times GSD + (b_{21} \times m_r + b_{22}))}$).

κ	a_{11}	a_{12}	a_2	b_{11}	b_{12}	b_{21}	b_{22}
0.1	5.70E-3	−3.70E-3	4.00E-2	−2.92E-1	8.32E-1	1.67E0	−3.50E0
0.3	2.23E-2	−7.80E-3	7.00E-2	−5.57E-1	1.39E0	2.26E0	−4.82E0
0.5	3.53E-2	9.00E-4	7.00E-2	−6.86E-1	1.70E0	2.56E0	−5.54E0
0.7	4.71E-2	7.20E-3	7.00E-2	−7.55E-1	1.88E0	3.25E0	−6.74E0
1.24	7.33E-2	2.23E-2	7.00E-2	−8.53E-1	2.17E0	2.94E0	−6.67E0

for a_1, a_2, b_1, and b_2. Combining Equations (12) and (13), the resultant κ_{sca} for polydisperse aerosols can be expressed as follows:

$$\kappa_{sca}(m_r, GSD, d_{g0}) = ((a_{11}m_r + a_{12})GSD + a_2) \times d_{g0}^{((b_{11}m_r+b_{12})\times GSD+(b_{21}m_r+b_{22}))} \quad (14)$$

From Equations (6) and (14), corresponding f(RH) can be given:

$$f(RH) = 1 + ((a_{11}m_r + a_{12})GSD + a_2) \times d_{g0}^{((b_{11}m_r+b_{12})\times GSD+(b_{21}m_r+b_{22}))} \frac{RH}{100 - RH} \quad (15)$$

The coefficients for resultant parameterization are summarized in Table 2 and Figure S1. The resultant analytic expression for κ_{sca} and f(RH) depend on the aerosol size distribution and refractive index for a given κ.

3. Results and discussion

Figure 3 shows κ_{sca} as a function of d_{g0} and GSD for different m_r. m_r of 1.4, 1.5, and 1.6 with κ of 0.5 was considered. As Figure 3 shows, κ_{sca} depends on size distribution. κ_{sca} decreases as d_{g0} and GSD increase. Figure 3 shows that κ_{sca} also depends on m_r. Figures 3a–c show κ_{sca} decreases as m_r increases, especially for small d_{g0}. This tendency is from the optical calculation of a complex function of refractive index, hygroscopicity, and size distribution (Contours of κ_{sca} can be seen in Figure S2). According to Jung et al. (2021), f(RH) from Mie calculations show f(RH) decreases as d_{g0} and GSD increase, and this is because of the size dependency of aerosol hygroscopicity. The size tendencies of κ_{sca} shown in Figure 3 are related to that of f(RH). Size-dependent κ_{sca}, with other κ values (0.1, 0.3, 0.7, and 1.24), are shown in Figures S3–S7, which show that the κ_{sca} decreases as κ decreases. As shown in Figure 3, the significant change in κ_{sca} is mainly for small GSD and d_{g0}.

In order to explicitly discuss the sensitivity of size distribution and refractive index on κ_{sca}, we calculated

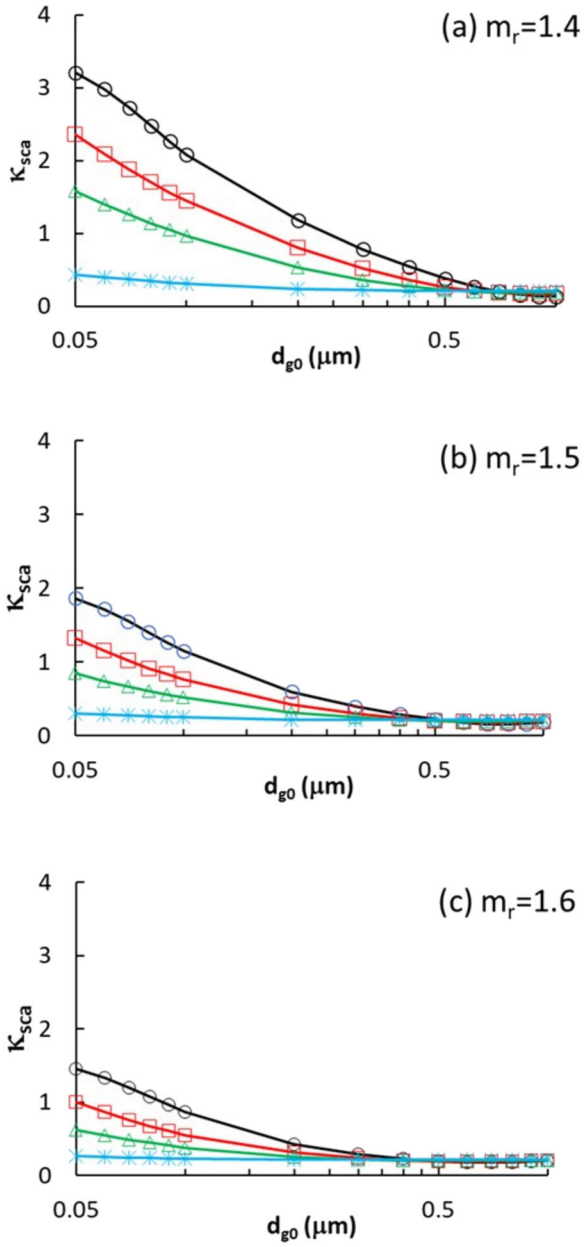

Figure 3. κ_{sca} as a function of d_{g0} with different GSDs at $\kappa = 0.5$, when (a) m_r=1.4, (b) m_r = 1.5, and (c) m_r = 1.6. (—○—: GSD = 1.3; —□—: GSD = 1.5; —△—: GSD = 1.7; —✳—: GSD = 2.5).

how κ_{sca} varies as a function of d_{g0}, GSD, and m_r. Table 3 shows how $\delta\kappa_{sca}/\delta lnd_{g0}$, $\delta\kappa_{sca}/\delta GSD$, and $\delta\kappa_{sca}/\delta m_r$ change in the range of d_{g0} of 0.05–1 μm, GSD of 1.3–2.5, and m_r of 1.35–1.6. As shown in Table 3, $\delta\kappa_{sca}/\delta lnd_{g0}$ becomes more negative as d_{g0} decreases. For example, $\delta\kappa_{sca}/\delta lnd_{g0}$ is −0.59, when d_{g0} ranges between 0.1 and 0.2 μm and −0.13 when d_{g0} ranges between 0.5 and 0.6 μm at GSD and m_r of 1.5 and 1.45, respectively. The negative $\delta\kappa_{sca}/\delta lnd_{g0}$ means κ_{sca} decreases as d_{g0} increases. The slope of decreasing κ_{sca} becomes stiffer at small d_{g0} and flatten as d_{g0} increases. $\delta\kappa_{sca}/\delta GSD$ and $\delta\kappa_{sca}/\delta m_r$ also shows

Table 3. Sensitivity of κ_{sca} with size-resolved parameter (GSD, d_{g0}) and refractive index (m_r).

(a) $\delta\kappa_{sca}/\delta$lndg0 ($\kappa = 0.5$, $m_r = 1.45$).

GSD Range (d_{g0}, μm)	1.3	1.5	1.7	1.9	2.1	2.3	2.5
0.05-0.06	−9.3E-01	−1.0E + 00	−6.7E-01	−4.1E-01	−2.6E-01	−1.7E-01	−1.2E-01
0.06-0.07	−1.2E + 00	−9.8E-01	−6.0E-01	−3.7E-01	−2.4E-01	−1.6E-01	−1.1E-01
0.07-0.08	−1.3E + 00	−9.0E-01	−5.5E-01	−3.4E-01	−2.2E-01	−1.4E-01	−9.9E-02
0.08-0.09	−1.3E + 00	−8.3E-01	−5.1E-01	−3.1E-01	−2.0E-01	−1.3E-01	−9.1E-02
0.09-0.1	−1.2E + 00	−7.7E-01	−4.7E-01	−2.9E-01	−1.9E-01	−1.2E-01	−8.4E-02
0.1-0.2	−9.1E-01	−5.9E-01	−3.6E-01	−2.2E-01	−1.4E-01	−8.9E-02	−5.8E-02
0.2-0.3	−6.2E-01	−4.0E-01	−2.4E-01	−1.4E-01	−7.8E-02	−4.5E-02	−2.6E-02
0.3-0.4	−4.7E-01	−3.0E-01	−1.6E-01	−8.1E-02	−4.1E-02	−2.0E-02	−9.0E-03
0.4-0.5	−4.0E-01	−2.1E-01	−9.6E-02	−4.3E-02	−1.8E-02	−6.0E-03	−3.4E-04
0.5-0.6	−3.3E-01	−1.3E-01	−4.8E-02	−1.6E-02	−3.3E-03	2.2E-03	4.0E-03
0.6-0.7	−2.3E-01	−6.2E-02	−1.3E-02	8.2E-04	5.4E-03	6.7E-03	5.8E-03
0.7-0.8	−1.1E-01	−2.7E-03	1.0E-02	1.1E-02	1.0E-02	8.9E-03	6.2E-03
0.8-0.9	2.0E-02	3.9E-02	2.4E-02	1.6E-02	1.3E-02	9.7E-03	5.7E-03
0.9-1.0	1.3E-01	6.2E-02	3.0E-02	1.9E-02	1.3E-02	9.7E-03	4.6E-03

(b) $\delta\kappa_{sca}/\delta$GSD ($\kappa = 0.5$, m_r=1.45).

d_{g0} (μm) Range (GSD)	0.05	0.1	0.5	1.0
1.3-1.5	−3.1E + 00	−2.2E + 00	−2.2E-01	−2.2E-01
1.5-1.7	−2.7E + 00	−1.5E + 00	−4.8E-02	−4.8E-02
1.7-1.9	−1.6E + 00	−8.6E-01	5.8E-04	5.8E-04
1.9-2.1	−9.2E-01	−4.8E-01	1.1E-02	1.1E-02
2.1-2.3	−5.3E-01	−2.7E-01	1.3E-02	1.3E-02
2.3-2.5	−3.2E-01	−1.6E-01	1.2E-02	1.2E-02

(c) $\delta\kappa_{sca}/\delta$m$_r$ ($\kappa = 0.5$, GSD = 1.5).

d_{g0} (μm) Range (m_r)	0.05	0.1	0.5	1.0
1.3-1.35	−1.4E + 01	−9.4E + 00	−1.2E + 00	1.3E-01
1.35-1.4	−9.4E + 00	−6.2E + 00	−7.0E-01	1.9E-01
1.4-1.45	−6.6E + 00	−4.3E + 00	−4.0E-01	1.9E-01
1.45-1.5	−4.8E + 00	−3.1E + 00	−2.2E-01	1.6E-01
1.5-1.55	−3.6E + 00	−2.4E + 00	−9.9E-02	1.1E-01
1.55-1.6	−2.8E + 00	−1.8E + 00	−1.9E-02	7.0E-02

a similar tendency. The slope of κ_{sca}, $\delta\kappa_{sca}/\delta GSD$, and $\delta\kappa_{sca}/\delta m_r$ are negative and flatten as GSD and m_r increase. $\delta\kappa_{sca}/\delta GSD$ is −2.2 when GSD ranges between 1.3–1.5 and −0.48 when GSD ranges between 1.9 and 2.1 at d_{g0} and m_r of 0.1 μm and 1.45, respectively. $\delta\kappa_{sca}/\delta m_r$ is −4.3 when m_r ranges between 1.4–1.45 and −1.8 when m_r ranges between 1.55 and 1.6 at d_{g0} and GSD of 0.1 μm and 1.5, respectively. These results show that the slope of κ_{sca} is closely related to the size distribution parameter as well as m_r, and more sensitive at small sizes with narrow distribution. Figure S8 shows these relationships graphically.

Figure 4 shows the comparison between the calculated κ_{sca}, obtained using Mie theory and the approximated κ_{sca} from Equation (12). The κ_{sca} at κ of 0.3 (Figure 4a) and 0.5 (Figure 4b) are shown and more comparisons with other κ values are shown in Figure S9. As Figure 4 shows, the analytically approximated κ_{sca} is comparable to Mie calculated κ_{sca}, with the slope of 0.98 and 0.94 for κ of 0.3 and 0.5, respectively. The approximation from this study is from statistical fitting based on Mie theory and the results show that the slope is underestimated for more hygroscopic aerosols (larger κ) compared with less hygroscopic aerosols. Tables S1–S5 compare the calculated and analytically approximated κ_{sca} for different κ values. The results showed that the obtained approximated expressions from this study were accurate, with an error of −21.3 − 16.4%, −25.8 − 22.6%, and −31.3 − 25.1%, for a κ of 0.1, 0.3, and 0.5, respectively, with GSD ranging from 1.3 to 2.5 and d_{g0} ranging from 0.05 to 1 μm. In our approach, we approximated the optical parameters, κ_{sca}, based on a 15-point approximation; however, the accuracy depends on the number of parameter fits. Tables S6–S10 and Figures S11–S15 compare the parameters and show how the accuracy of estimation changes when the number of parameterization points changes from 15 to 4. Here, the points are the number of values used for linear regressions.

κ_{sca} and κ are related, but substantially different parameters that can be coupled using Mie theory and the particle size distribution function (Brock et al. 2016).

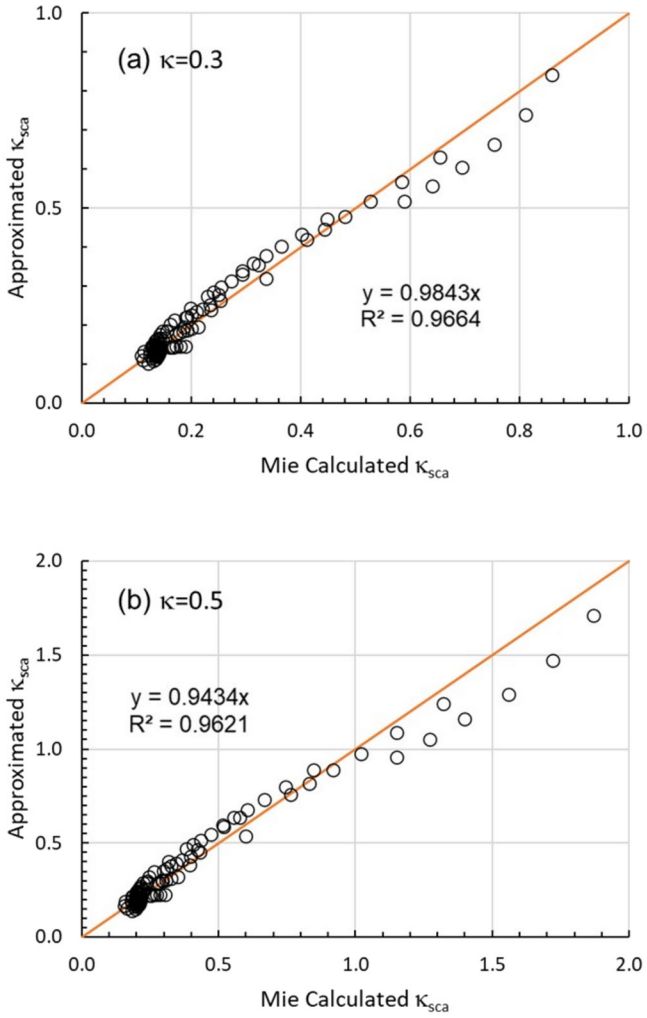

Figure 4. Comparison between the Mie calculated and approximated κ_{sca} for m_r=1.5 in the range of GSD of 1.3–2.5 and d_{g0} of 0.05 ~ 1 μm, when (a) $\kappa = 0.3$ and (b) $\kappa = 0.5$.

Figure 5 shows the κ_{sca}/κ as a function of d_{g0} and GSD with κ values of 0.3 and 0.5. The m_r of 1.5 is considered. Other results at κ values of 0.1, 0.7, and 1.24 are shown in Figure S10. As Figure 5 shows, the κ_{sca}/κ ratio decreases as the d_{g0} and GSD increase. This means that the κ_{sca}/κ ratio decreases as the polydispersity of aerosol size distribution increases. This might be because large GSD includes larger particles compared to that of smaller GSD, which lowers the κ_{sca}. The optical properties of hygroscopic polydispersed aerosol can be obtained from Mie theory.

Comparing κ_{sca}/κ with different κ values shows that the κ_{sca}/κ ratio increases as κ increases for small d_{g0}. Figure 5 also shows that the currently obtained approximation agrees well with Mie calculation results for polydisperse aerosol size tendencies. It should be noted that the range of κ_{sca}/κ depends on d_{g0}, m_r, and GSD. A close relationship between κ_{sca} and κ was reported by several observational studies (Brock et al. 2016; Kuang et al. 2017; Yu et al. 2018). Based on κ derived from aerosol size distributions and f(RH) measurements, Kuang et al. (2017) estimated κ_{sca}/κ from a site in the North China Plains to range between 0.55 and 0.81, which varies with a particle size distribution, with smaller particles having relatively higher ratios. According to Brock et al. (2016), κ_{sca}/κ for a typical accumulation mode is expected to be 0.5 to 1, which is similar to that in the current study when the geometric mean diameter is in the range of 0.1–0.2 μm. The direct comparison of κ_{sca}/κ between observation and this study was unavailable because of the lack of data regarding aerosol size distribution. Our theoretical study quantitively determined the κ_{sca}/κ ratio for polydisperse aerosols using analytic formulae.

Figure 6 compares f(RH) as a function of RH between numerically calculated and analytically approximated solutions. A κ value of 0.5 was considered for different size distributions with d_{g0} of 0.1 and 0.7 μm with a GSD of 1.5 and 1.9, respectively. The

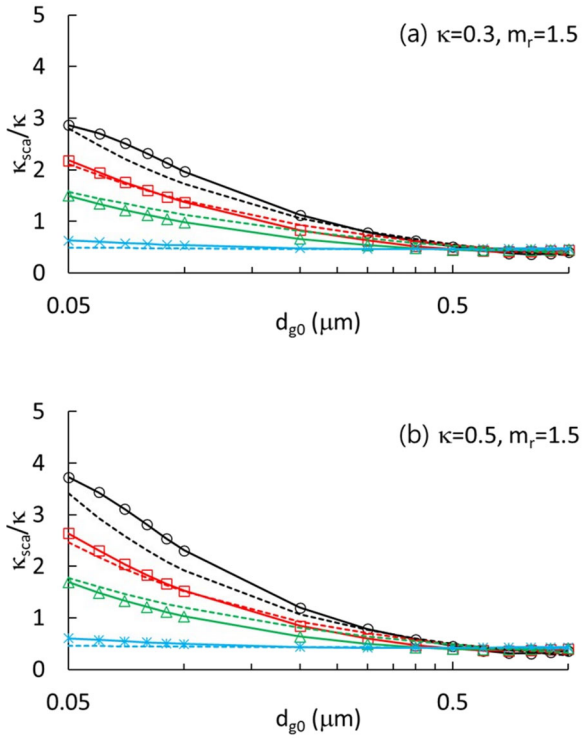

Figure 5. Comparisons between Mie calculated and approximated κ_{sca}/κ as a function of d_{g0} with different GSDs, when (a) $\kappa = 0.3$ and (b) $\kappa = 0.5$. (—○—: GSD = 1.3; —□—: GSD = 1.5; —△—: GSD = 1.7; —✳—: GSD = 2.5, solid line; Mie calculation, dashed line: Approximation).

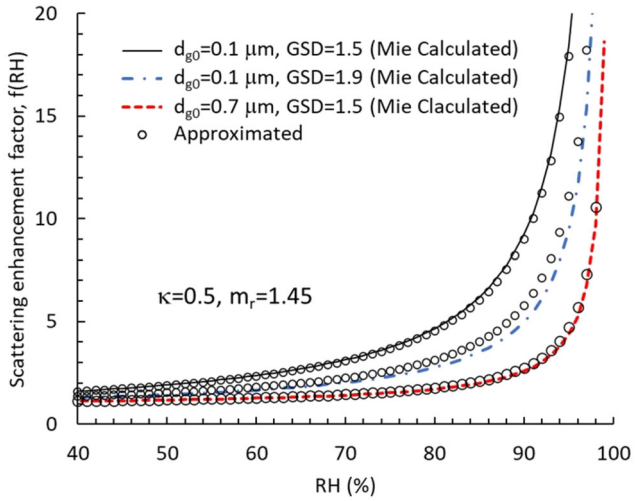

Figure 6. Comparisons of the f(RH) between Mie-calculated and approximated solutions as a function of RH for different size distributions.

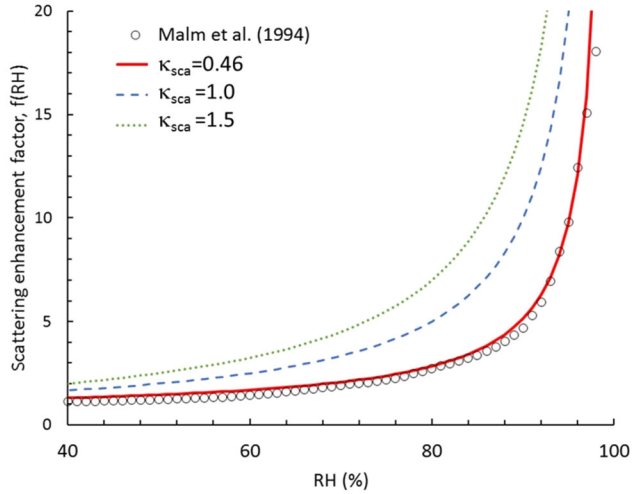

Figure 7. Comparisons of the f(RH) between Malm et al. (1994) and different κ_{sca} as a function of RH.

circle symbol stands for approximated values, and solid, dash-dotted, and dashed lines represent Mie calculated values at different size distributions. As Figure 6 shows, the Mie-calculated and approximated values are consistent with each other. Figure 6 also shows that the f(RH) depends on size distribution. Among the given size distribution conditions, the results show higher f(RH) at d_{g0} of 0.1 μm than at d_{g0} of 0.7 μm. It also shows higher f(RH) at GSD of 1.5 than at GSD of 1.9 when d_{g0} is 0.1 μm. From these results, we can infer that f(RH) decreases as GSD and d_{g0} increase. Previous studies, including the results for ammonium sulfate from Malm et al. (1994), do not consider size distribution in estimating f(RH).

Figure 7 shows the comparisons of the f(RH) between Malm et al. (1994) and different κ_{sca} as a function of RH for κ_{sca} of 0.46, 1.0, and 1.5. As Figure 7 shows, f(RH) at large κ_{sca} has a larger f(RH). The current study shows f(RH) is size-dependent and different with κ_{sca}. Thus, the size distribution should be considered in estimating f(RH). The analytic expression from this study shows that κ_{sca} can be quantitively expressed as a function of d_{g0} and GSD. The obtained κ_{sca} and f(RH) can be applied three-dimensionally. The detailed descriptions for three-dimensional model simulation are provided in Section 2.3.

The spatial comparison of κ_{sca} and f(RH) of ammonium sulfate aerosol between the reconstructed expression from Malm et al. (1994) and our parameterization was made over East Asia in Figure 8. While the κ_{sca} of ammonium sulfate in the reconstructed expression from Malm et al. (1994) is a constant (κ_{sca} ~0.46), regardless of aerosol size distribution, the newly derived κ_{sca} in Equation (14) has a more dynamic spatial distribution. For example, the new κ_{sca} shows a lower value over the Northwest Pacific Ocean. Upon comparing the size distribution parameters, d_{g0} and GSD at accumulation mode between the continent and ocean, the d_{g0} is smaller, and GSD is larger over the ocean than those over the

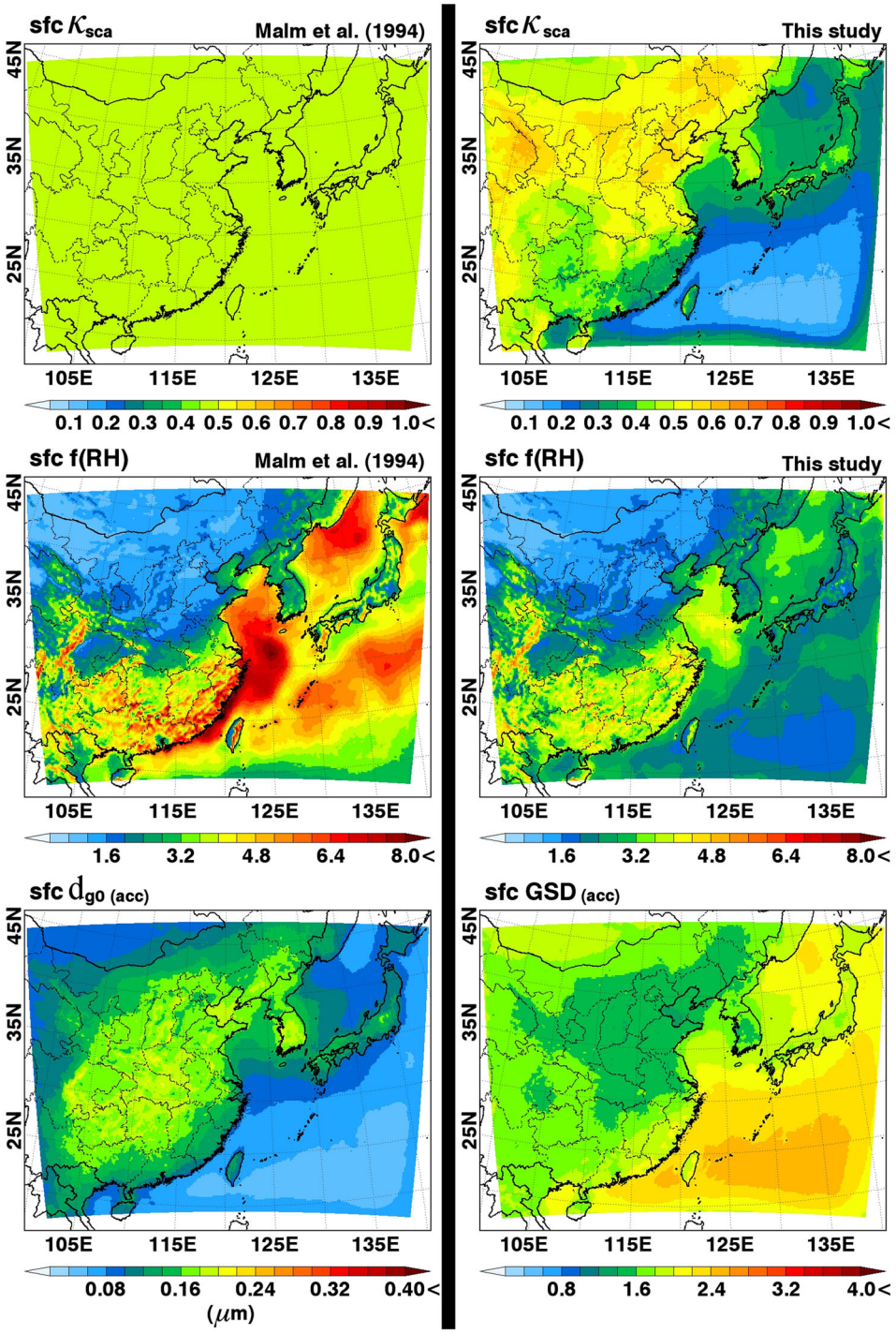

Figure 8. Comparisons of the spatial distribution of κ_{sca} and f(RH) between the accumulation mode ammonium sulfate of the reconstructed expression in Malm et al. (1994) and that in this study during KORUS-AQ periods (Bottom panel shows d_{g0} and GSD of accumulation mode aerosol size distribution).

continent. According to Figure 8, κ_{sca} decreases as d_{g0} and GSD increase. The lower values of κ_{sca} and f(RH) around the sea are attributed to the high GSD value compared with that over the continental region. Figure 8 also shows that the currently derived f(RH) yields lower values compared with f(RH) from Malm et al. (1994). The degree of discrepancies between Malm's reconstructed approach and the current work is attributed to aerosol size distributions because the currently derived expression considers the size distribution using the d_{g0} and GSD.

Figure 9 shows the vertical distributions of κ_{sca} and f(RH) of ammonium sulfate aerosol from the reconstructed expression of Malm et al. (1994) and our

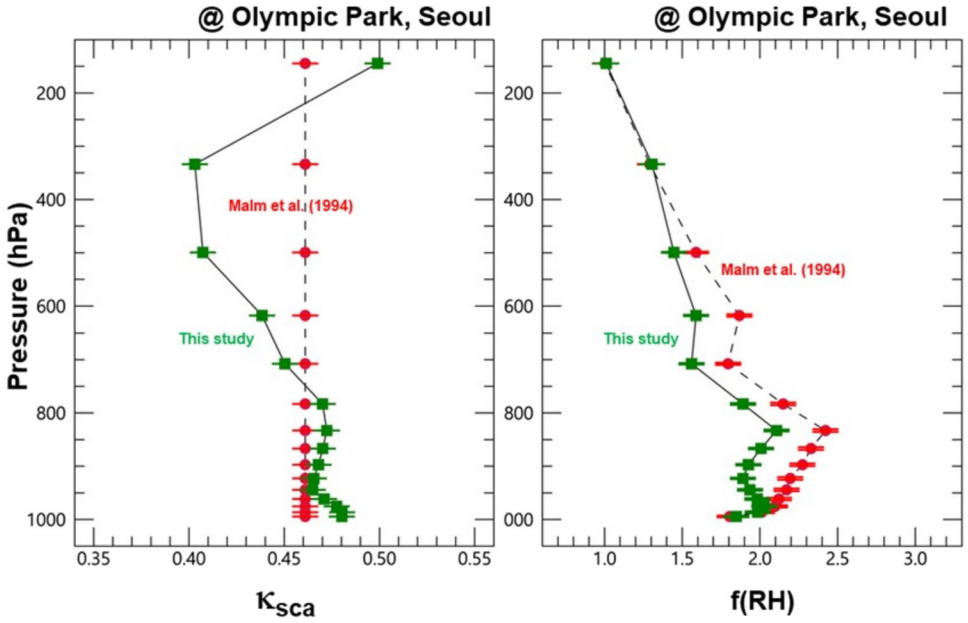

Figure 9. Comparisons of the vertical distribution of κ_{sca} and f(RH) between the accumulation mode ammonium sulfate of the reconstructed expression in Malm et al. (1994) and that in this study during KORUS-AQ periods.

parameterization. Similar to the spatial distributions in Figure 8, while the vertical distribution of κ_{sca} from Malm et al. (1994) is also constant, the currently derived κ_{sca} shows different vertical distributions depending on size distribution. Despite similar vertical distributions, the vertical distributions between both f(RH) are similar, and the newly derived f(RH) is smaller than the reconstructed expression of Malm et al. (1994).

4. Conclusions

In this study, approximated analytic expressions approximating κ_{sca} and f(RH) were developed for polydisperse aerosol sizes at a d_{g0} of 0.05–1 μm with GSD ranging from 1.3 to 2.5. Dry aerosol refractive indices of 1.35–1.6 with κ values of 0.1, 0.3, 0.5, 0.7, and 1.24 were considered. Results were compared with the Mie-calculated results in the size range considered in this study.

κ_{sca} could be quantitively expressed at a given κ as a function of d_{g0} and GSD of a lognormal distribution along with the refractive index. Our results showed that the κ_{sca} decreases as d_{g0}, GSD, and m_r increase at a given κ. Finally, the comparison between the f(RH) of the reconstructed method of Malm et al. (1994) and that in this study was conducted for the results during the KORUS-AQ intensive observation period using CMAQ simulations. Compared with the f(RH) of the reconstructed method by Malm et al. (1994), which do not consider size distribution, the newly developed f(RH) parameterization using the κ_{sca} for polydisperse aerosol shows significant variations of the f(RH), depending on particle size distribution.

The current aerosol module in the CMAQ model has been developed in three lognormal modes (Aitken, accumulation, and coarse) to minimize the computational burden in aerosol calculation. Nevertheless, high-resolved 3-D CTM simulation is computationally expensive. Therefore, the application of our parameterization to the CMAQ output can be efficiently used to express size-dependent aerosol optical properties.

In this study, we excluded the hygroscopic growth of absorbing aerosol as most absorbing aerosols do not have hygroscopic properties and assumed that scattering enhancement is due to the hygroscopic growth. However, it should be noted that some absorbing particles, such as brown carbon and black carbon with a core-shell aerosol mixture, also have hygroscopicity and imaginary refractive index cannot be neglected (Bain et al. 2019; Freedman et al. 2009; Zeng et al. 2019). From a methodological point of view, our approach can be extended to a case where the imaginary part of the refractive index is not negligible under the assumption of a fully homogeneous internal mixture. The resultant approximated equation should be expressed with imaginary refractive index-related parameters. For core-shell mixtures, other variables, such as coating thickness and refractive index of core and shell particles, should be considered separately. It should also be noted that our methodology

can be extended to other wavelengths. The coefficients might be different for different wavelengths.

This study disregards Kelvin effects (Park and Lee 2000). The Kelvin effect for small particles will be included in future studies. This study could not compare κ_{sca} directly with previously reported values based on observation because of the lack of information regarding aerosol size distribution, and will be also explored in a future study.

Finally, the expression obtained from this study can be easily used to quantify the effects of aerosol size distribution for studying hygroscopicity and the relation between aerosol optical and physico-chemical properties. This approach can be efficiently used in 3D models, as it requires simplified parameterization with a reduced computational burden.

Nomenclature

Abbreviations

GR	growth factor
RH	relative humidity
f(RH)	aerosol light scattering enhancement factor
κ	single hygroscopicity parameter
κ_{sca}	single hygroscopic optical parameter

Funding

This study was supported by the FRIEND (Fine Particle Research Initiative in East Asia Considering National Differences) Project through the National Research Foundation of Korea (NRF) funded by the Ministry of Science and ICT (grant number 2020M3G1A1114617); the National Research Foundation of Korea Grant from the Korean Government (MSIT) (grant number NRF2021M1A5A1065672/KOPRI-PN23011, NRF2021R1F1A1046878, NRF2020R1A2C1003215, and NRF2023R1A2C1002367). This research was also supported by Basic Science Research Program through the National Research Foundation of Korea (NRF), funded by the Ministry of Education (no. 2020R1A6A1A03044834).

References

Almeida, G. P., A. T. Bittencourt, M. S. Evangelista, M. S. Vieira-Filho, and A. Fornaro. 2019. Characterization of aerosol chemical composition from urban pollution in Brazil and its possible impacts on the aerosol hygroscopicity and size distribution. *Atmos. Environ.* 202:149–59. doi:10.1016/j.atmosenv.2019.01.024.

Bain, A., A. Rafferty, and T. C. Preston. 2019. The wavelength-dependent complex refractive index of hygroscopic aerosol particles and other aqueous media: An effective oscillator model. *Geophys. Res. Lett.* 46 (17-18):10636–10645. doi:10.1029/2019GL084568.

Binkowski, F. S. 1999. *Chapter 10: Aerosols in MODELS-3.* Washington, DC: CMAQ.

Binkowski, F. S., and S. J. Roselle. 2003. Models-3 Community Multiscale Air Quality (CMAQ) model aerosol component 1. Model description. *J. Geophys. Res.* 108 (D6):4183. doi:10.1029/2001JD001409.

Bohren, C. F., and D. R. Huffman. 1983. *Absorption and scattering of light by small particles.* New York: John Wiley & Sons.

Brock, C. A., N. L. Wagner, B. E. Anderson, A. R. Attwood, A. Beyersdorf, P. Campuzano-Jost, A. G. Carlton, D. A. Day, G. S. Diskin, T. D. Gordon, et al. 2016. Aerosol optical properties in the southeastern United States in summer – Part 1: Hygroscopic growth. *Atmos. Chem. Phys.* 16 (8):4987–5007. doi:10.5194/acp-16-4987-2016.

Byun, D. W., and K. L. Schere. 2006. Review of the governing equations, computational algorithms, and other components of the models-3 community multiscale air quality (CMAQ) modeling system. *Appl. Mech. Rev.* 59 (2):51–77. doi:10.1115/1.2128636.

Chen, J., C. S. Zhao, N. Ma, and P. Yan. 2014. Aerosol hygroscopicity parameter derived from the light scattering enhancement factor measurements in the North China Plain. *Atmos. Chem. Phys.* 14 (15):8105–8118. doi:10.5194/acp-14-8105-2014.

Covert, D. S., R. J. Charlson, and N. C. Ahlquist. 1972. A study of the relationship of chemical composition and humidity to light scattering by aerosols. *J. Appl. Meteor.* 11 (6):968–976. doi:10.1175/1520-0450(1972)011<0968:ASOTRO>2.0.CO;2.

Crawford, J. H., J. Y. Ahn, J. Al-Saadi, L. Chang, L. K. Emmons, J. Kim, G. Lee, J. H. Park, R. J. Park, J. H. Woo, et al. 2021. The Korea–United States Air Quality (KORUS-AQ) field study. *Elementa (Wash DC).* 9 (1):1–27. doi:10.1525/elementa.2020.00163.

Cuevas-Robles, A., N. Soltani, B. Keshavarzi, J. S. Youn, A. B. MacDonald, and A. Sorooshian. 2021. Hygroscopic and chemical properties of aerosol emissions at a major mining facility in Iran: Implications for respiratory deposition. *Atmos. Pollut. Res.* 12 (3):292–301. doi:10.1016/j.apr.2020.12.015.

Dubovik, O., B. Holben, T. F. Eck, A. Smirnov, Y. J. Kaufman, M. D. King, D. Tanré, and I. Slutsker. 2002. Variability of absorption and optical properties of key aerosol types observed in worldwide locations. *J. Atmos. Sci.* 59 (3):590–608. doi:10.1175/1520-0469(2002)059<0590:VOAAOP>2.0.CO;2.

Eichler, H., Y. F. Cheng, W. Birmili, A. Nowak, A. Wiedensohler, E. Brüggemann, T. Gnauk, H. Herrmann, D. Althausen, and A. Ansmann. 2008. Hygroscopic properties and extinction of aerosol particles at ambient relative humidity in South-Eastern China. *Atmos. Environ.* 42 (25):6321–6334. doi:10.1016/j.atmosenv.2008.05.007.

Erlick, C., J. P. D. Abbatt, and Y. Rudich. 2011. How different calculations of the refractive index affect estimates of the radiative forcing efficiency of ammonium sulfate aerosols. *J. Atmos. Sci.* 68 (9):1845–1852. doi:10.1175/2011JAS3721.1.

Fard, M. M., U. K. Krieger, and T. Peter. 2018. Shortwave radiative impact of liquid–liquid phase separation in brown carbon aerosols. *Atmos. Chem. Phys.* 18 (18):13511–13530. doi:10.5194/acp-18-13511-2018.

Ferrare, R. A., S. H. Melfi, D. N. Whiteman, K. D. Evans, M. Poellot, and Y. J. Kaufman. 1998. Raman lidar measurements of aerosol extinction and backscattering—2. Derivation of aerosol real refractive index, single-scattering albedo, and humidification factor using Raman lidar

and aircraft size distribution measurements. *J. Geophys. Res.* 103 (D16):19673–19689. doi:10.1029/98JD01647.

Freedman, M. A., C. A. Hasenkopf, M. R. Beaver, and M. A. Tolbert. 2009. Optical properties of internally mixed aerosol particles composed of dicarboxylic acids and ammonium sulfate. *J. Phys. Chem. A.* 113 (48): 13584–13592. PMID: 19877658. doi:10.1021/jp906240y.

Guyon, P., O. Boucher, B. Graham, J. Beck, O. L. Mayol-Bracero, G. C. Roberts, W. Maenhaut, P. Artaxo, and M. O. Andreae. 2003. Refractive index of aerosol particles over the Amazon tropical forest during LBA-EUSTACH 1999. *J. Aerosol Sci.* 34 (7):883–907. doi:10.1016/S0021-8502(03)00052-1.

Han, K. M., C. H. Jung, R. S. Park, S. Y. Park, S. Lee, M. Kulmala, T. Petäjä, G. Karasiński, P. Sobolewski, Y. J. Yoon, et al. 2021. Data assimilation of AOD and estimation of surface particulate matters over the Arctic. *Appl. Sci.* 11 (4):1959. doi:10.3390/app11041959.

Haywood, J., and O. Boucher. 2000. Estimates of the direct and indirect radiative forcing due to tropospheric aerosols: A review. *Rev. Geophys.* 38 (4):513–543. doi:10.1029/1999RG000078.

He, Q., N. Bluvshtein, L. Segev, D. Meidan, J. M. Flores, S. S. Brown, W. Brune, and Y. Rudich. 2018. Evolution of the complex refractive index of secondary organic aerosols during atmospheric aging. *Environ. Sci. Technol.* 52 (6):3456–65. doi:10.1021/acs.est.7b05742.

Horvath, H., M. Kasaharat, and P. Pesava. 1996. The size distribution and composition of the atmospheric aerosol at a rural and nearby urban location. *J. Aerosol Sci.* 27 (3):417–435. doi:10.1016/0021-8502(95)00546-3.

Jung, C. H., Y. J. Yoon, J. Um, S. S. Lee, K. M. Han, H. J. Shin, J. Y. Lee, and Y. P. Kim. 2021. Approximated expression of the hygroscopic growth factor for polydispersed aerosols. *J. Aerosol Sci.* 151:105670. doi:10.1016/j.jaerosci.2020.105670.

Junge, C., and E. McLaren. 1971. Relationship of cloud nuclei spectra to aerosol size distribution and composition. *J. Atmos. Sci.* 28 (3):382–390. doi:10.1175/1520-0469(1971)028<0382:ROCNST>2.0.CO;2.

Jurányi, Z., and R. Weller. 2019. One year of aerosol refractive index measurement from a coastal Antarctic site. *Atmos. Chem. Phys.* 19 (22):14417–14430. doi:10.5194/acp-19-14417-2019.

Koike, M., N. Moteki, P. Khatri, T. Takamura, N. Takegawa, Y. Kondo, H. Hashioka, H. Matsui, A. Shimizu, and N. Sugimoto. 2014. Case study of absorption aerosol optical depth closure of black carbon over the East China Sea. *J. Geophys. Res. Atmos.* 119 (1):122–136. doi:10.1002/2013JD020163.

Kreidenweis, S. M., M. D. Petters, and P. J. DeMott. 2008. Single-parameter estimates of aerosol water content. *Environ. Res. Lett.* 3 (3):035002. doi:10.1088/1748-9326/3/3/035002.

Kuang, Y., C. Zhao, J. Tao, Y. Bian, N. Ma, and G. Zhao. 2017. A novel method for deriving the aerosol hygroscopicity parameter based only on measurements from a humidified nephelometer system. *Atmos. Chem. Phys.* 17 (11):6651–6662. doi:10.5194/acp-17-6651-2017.

Lagrosas, N., G. Bagtasa, N. Manago, and H. Kuze. 2019. Influence of ambient relative humidity on seasonal trends of the scattering enhancement factor for aerosols in Chiba, Japan. *Aerosol Air Qual. Res.* 19 (8):1856–1871. doi:10.4209/aaqr.2018.07.0267.

Laskina, O. V., H. S. Morris, J. R. Grandquist, Z. Qin, E. A. Stone, A. V. Tivanski, and V. H. Grassian. 2015. Size matters in the water uptake and hygroscopic growth of atmospherically relevant multicomponent aerosol particles. *J. Phys. Chem. A.* 119 (19):4489–4497. doi:10.1021/jp510268p.

Levin, E. J. T., A. J. Prenni, B. B. Palm, D. A. Day, P. Campuzano-Jost, P. M. Winkler, S. M. Kreidenweis, P. J. DeMott, J. L. Jimenez, and J. N. Smith. 2014. Size-resolved aerosol composition and its link to hygroscopicity at a forested site in Colorado. *Atmos. Chem. Phys.* 14 (5):2657–2667. doi:10.5194/acp-14-2657-2014.

Levoni, C., M. Cervino, R. Guzzi, and F. Torricella. 1997. Atmospheric aerosol optical properties: A database of radiative characteristics for different components and classes. *Appl. Opt.* 36 (30):8031–8041. doi:10.1364/Ao.36.008031.

Li, J., Z. Han, and R. Zhang. 2014. Influence of aerosol hygroscopic growth parameterization on aerosol optical depth and direct radiative forcing over East Asia. *Atmos. Res* 140-141:14–27. doi:10.1016/j.atmosres.2014.01.013.

Malm, W. C., J. F. Sisler, D. Huffman, R. A. Eldred, and T. A. Cahill. 1994. Spatial and seasonal trends in particle concentration and optical extinction in the United States. *J. Geophys. Res.* 99 (D1):1347–1370. doi:10.1029/93JD02916.

McFiggans, G., P. Artaxo, U. Baltensperger, H. Coe, M. C. Facchini, G. Feingold, S. Fuzzi, M. Gysel, A. Laaksonen, U. Lohmann, et al. 2006. The effect of physical and chemical aerosol properties on warm cloud droplet activation. *Atmos. Chem. Phys.* 6 (9):2593–2649. doi:10.5194/acp-6-2593-2006.

Mico, S., A. Deda, E. Tsaousi, M. Alushllari, and P. Pomonis. 2019. Complex refractive index of aerosol samples. *AIP Conf. Proc.* 2109:060002. doi:10.1063/1.5110120.

Moise, T., J. M. Flores, and Y. Rudich. 2015. Optical properties of secondary organic aerosols and their changes by chemical processes. *Chem. Rev.* 115 (10):4400–4439. doi:10.1021/cr5005259.

Molnár, A., K. Imre, Z. Ferenczi, G. Kiss, and A. Gelencsér. 2020. Aerosol hygroscopicity: Hygroscopic growth proxy based on visibility for low-cost PM monitoring. *Atmos. Res.* 236:104815. doi:10.1016/j.atmosres.2019.104815.

Park, S. H., and K. W. Lee. 2000. Condensational growth of polydisperse aerosol for the entire particle size range. *Aerosol Sci. Technol.* 33 (3):222–227. doi:10.1080/027868200416213.

Petters, M. D., and S. M. Kreidenweis. 2007. A single parameter representation of hygroscopic growth and cloud condensation nucleus activity. *Atmos. Chem. Phys.* 7 (8): 1961–1971. doi:10.5194/acp-7-1961-2007.

Pitchford, M., W. Maim, B. Schichtel, N. Kumar, D. Lowenthal, and J. Hand. 2007. Revised algorithm for estimating light extinction from IMPROVE particle speciation data. *J. Air Waste Manag. Assoc.* 57 (11):1326–1336. doi:10.3155/1047-3289.57.11.1326.

Seinfeld, J. H., and S. N. Pandis. 2016. *Atmospheric chemistry and physics: From air pollution to climate change*. Hoboken, NJ: John Wiley & Sons.

Shingler, T., E. Crosbie, A. Ortega, M. Shiraiwa, A. Zuend, A. Beyersdorf, L. Ziemba, B. Anderson, L. Thornhill,

A. E. Perring, et al. 2016. Airborne characterization of subsaturated aerosol hygroscopicity and dry refractive index from the surface to 6.5 km during the SEAC4RS campaign. *JGR Atmos.* 121 (8):4188–4210. doi:10.1002/2015JD024498.

Shulman, M. L., M. C. Jacobson, R. J. Carlson, R. E. Synovec, and T. E. Young. 1996. Dissolution behavior and surface tension effects of organic compounds in nucleating cloud droplets. *Geophys. Res. Lett.* 23 (3):277–280. doi:10.1029/95GL03810.

Sorooshian, A., S. M. Murphy, S. Hersey, H. Gates, L. T. Padro, A. Nenes, F. J. Brechtel, H. Jonsson, R. C. Flagan, and J. H. Seinfeld. 2008. Comprehensive airborne characterization of aerosol from a major bovine source. *Atmos. Chem. Phys.* 8 (17):5489–5520. doi:10.5194/acp-8-5489-2008.

Stevens, R., and A. A. Dastoor. 2019. A Review of the representation of aerosol mixing state in atmospheric models. *Atmosphere.* 10 (4):168. doi:10.3390/atmos10040168.

Stokes, R. H., and R. A. Robinson. 1966. Interactions in aqueous nonelectrolyte solutions. I. Solute-solvent equilibria. *J. Phys. Chem.* 70 (7):2126–2131. doi:10.1021/j100879a010.

Titos, G., A. Cazorla, P. Zieger, E. Andrews, H. Lyamani, M. J. Granados-Muñoz, F. J. Olmo, and L. Alados-Arboledas. 2016. Effect of hygroscopic growth on the aerosol light-scattering coefficient: A review of measurements, techniques and error sources. *Atmos. Environ.* 141:494–507. doi:10.1016/j.atmosenv.2016.07.021.

Topping, D. O., G. B. McFiggans, and H. Coe. 2005. A curved multi-component aerosol hygroscopicity model framework: Part 1 – Inorganic compounds. *Atmos. Chem. Phys.* 5 (5):1205–1222. doi:10.5194/acp-5-1205-2005.

Wang, W., and M. J. Rood. 2008. Real refractive index: Dependence on relative humidity and solute composition with relevancy to atmospheric aerosol particles. *J. Geophys. Res.* 113 (D23):D23305. doi:10.1029/2008JD010165.

Wang, X., X. J. Shen, J. Y. Sun, X. Y. Zhang, Y. Q. Wang, Y. M. Zhang, P. Wang, C. Xia, X. F. Qi, and J. T. Zhong. 2018. Size-resolved hygroscopic behavior of atmospheric aerosols during heavy aerosol pollution episodes in Beijing in December 2016. *Atmos. Environ.* 194:188–197. doi:10.1016/j.atmosenv.2018.09.041.

Wexler, A. S., and S. L. Clegg. 2002. Atmospheric aerosol models for systems including the ions H^+, NH_4, Na_+, SO_4^{2-}, NO_3^-, Cl^-, Br^- and H_2O. *J. Geophys. Res.* 107 (D14):4207. doi:10.1029/2001JD000451.

Yao, Y., J. H. Curtis, J. Ching, Z. Zheng, and N. Riemer. 2022. Quantifying the effects of mixing state on aerosol optical properties. *Atmos. Chem. Phys.* 22 (14):9265–9282. doi:10.5194/acp-22-9265-2022.

Yu, Y., C. Zhao, Y. Kuang, J. Tao, G. Zhao, C. Shen, and W. Xu. 2018. A parameterization for the light scattering enhancement factor with aerosol chemical compositions. *Atmos. Environ.* 191:370–377. doi:10.1016/j.atmosenv.2018.08.016.

Zdanovskii, A. B. 1948. New methods for calculating solubilities of electrolytes in multicomponent systems. *Zhur Fiz. Khim.* 22:1475–1485.

Zeng, C., C. Liu, J. Li, B. Zhu, Y. Yin, and Y. Wang. 2019. Optical properties and radiative forcing of aged BC due to hygroscopic growth: Effects of the aggregate structure. *J. Geophys. Res. Atmos.* 124 (8):4620–4633. doi:10.1029/2018JD029809.

Zhang, F., Y. Li, Z. Li, L. Sun, R. Li, C. Zhao, P. Wang, Y. Sun, X. Liu, J. Li, et al. 2014. Aerosol hygroscopicity and cloud condensation nuclei activity during the AC3 Exp campaign: Implications for cloud condensation nuclei parameterization. *Atmos. Chem. Phys.* 14 (24):13423–13437. doi:10.5194/acp-14-13423-2014.

Zhao, P. S., S. S. Ge, J. Su, J. Ding, and Y. Kuang. 2022. Relative humidity dependence of hygroscopicity parameter of ambient aerosols. *JGR Atmos.* 127 (8):e2021JD035647. doi:10.1029/2021JD035647.

Zieger, P., R. Fierz-Schmidhauser, M. Gysel, J. Ström, S. Henne, K. E. Yttri, U. Baltensperger, and E. Weingartner. 2010. Effects of relative humidity on aerosol light scattering in the Arctic. *Atmos. Chem. Phys.* 10 (8):3875–3890. doi:10.5194/acp-10-3875-2010.

Zieger, P., R. Fierz-Schmidhauser, E. Weingartner, and U. Baltensperger. 2013. Effects of relative humidity on aerosol light scattering: Results from different European sites. *Atmos. Chem. Phys.* 13 (21):10609–10631. doi:10.5194/acp-13-10609-2013.